The Astrophysical Journal, 793:56 (14pp), 2014 September 20 doi:10.1088/0004-637X/793/1/56

ACCRETION AND OUTFLOW IN THE PROPLYD-LIKE OBJECTS NEAR CYGNUS OB2

M. G. Guarcello[1,2], J. J. Drake[2], N. J. Wright[2,3], D. García-Alvarez[4,5,6], and K. E. Kraemer[7]
[1] INAF–Osservatorio Astronomico di Palermo, Piazza del Parlamento 1, I-90134 Palermo, Italy
[2] Smithsonian Astrophysical Observatory, MS-67, 60 Garden Street, Cambridge, MA 02138, USA
[3] CAR/STRI, University of Hertfordshire, College Lane, Hatfield AL10 9AB, UK
[4] Dpto. de Astrofísica, Universidad de La Laguna, E-38206 E-La Laguna, Tenerife, Spain
[5] Grantecan CALP, E-38712 Breña Baja, La Palma, Spain
[6] Instituto de Astrofísica de Canarias, E-38205 La Laguna, Tenerife, Spain
[7] Institute for Scientific Research, Boston College, Kenny Cottle L106B, Newton, MA 02459-1161, USA
Received 2014 April 8; accepted 2014 July 29; published 2014 September 5

ABSTRACT

Cygnus OB2 is the most massive association within 2 kpc from the Sun, hosting hundreds of massive stars, thousands of young low mass members, and some sights of active star formation in the surrounding cloud. Recently, 10 photoevaporating proplyd-like objects with tadpole-shaped morphology were discovered in the outskirts of the OB association, approximately 6–14 pc away from its center. The classification of these objects is ambiguous, being either evaporating residuals of the parental cloud that are hosting a protostar inside or disk-bearing stars with an evaporating disk, such as the evaporating proplyds observed in the Trapezium Cluster in Orion. In this paper, we present a study based on low-resolution optical spectroscopic observations made with the Optical System for Imaging and low Resolution Integrated Spectroscopy, mounted on the 10.4 m Gran Telescopio CANARIAS, of two of these protostars. The spectrum of one of the objects shows evidence of accretion but not of outflows. In the latter object, the spectra show several emission lines indicating the presence of an actively accreting disk with outflow. We present estimates of the mass loss rate and the accretion rate from the disk, showing that the former exceeds the latter as observed in other known objects with evaporating disks. We also show evidence of a strong variability in the integrated flux observed in these objects as well as in the accretion and outflow diagnostics.

Key words: stars: formation – stars: mass-loss – stars: pre-main sequence – stars: protostars

Online-only material: color figure

1. INTRODUCTION

Star formation in our Galaxy occurs in a variety of environments, with one of the main modes being in clusters hosting OB stars, and then characterized by an intense UV radiation field. In the past decade, several works have been focused on the understanding of how the evolution of circumstellar disks and the processes of star and planet formation are affected by an intense local UV field (Johnstone et al. 1998; Adams et al. 2004; Throop & Bally 2005; Guarcello et al. 2010).

In low-mass environments, characterized by a small number of massive stars and a weak local UV field, disks are observed to dissipate in less than 10 Myr. In such an environment, the fraction of cluster members holding an inner disk declines exponentially with an *e*-folding time of 2.5 Myr (Mamajek 2009).

In more massive environments, the hosted OB stars, despite their short lifetimes, have a strong impact on the evolution of the parental cloud, and on nearby young protostars and their circumstellar disks. The intense UV and X-ray radiation from OB stars ionizes the surrounding cloud, turning it into a H II region and clearing a cavity delimited by an expanding ionization front (Whitworth 1979). When the expanding front sweeps over local overdensities in the cloud, a residual evaporating globule of gas (called "Evaporating Gaseous Globules," EGGs) can be produced (Hester et al. 1996). The possibility that EGGs can actually be collapsing and forming one or more protostars in their center has been debated. For instance, in the Eagle Nebula, hosting tens of OB stars, only 15% of the 73 EGGs observed close to the Pillars of Creation have protostars in their centers (McCaughrean & Andersen 2002).

In general, new stars form in the contracting molecular cloud during the expansion of the ionization front created by the massive stars (Elmegreen 2011). As soon as these young stars emerge from the expanding front, they are exposed to the ionizing radiation emitted by the massive stars. As directly observed in the Trapezium in Orion (Henney & O'Dell 1999) using the *Hubble Space Telescope* (*HST*), where an intense UV field is created by the O6V star Θ^1 Ori, disks irradiated by massive stars can be quickly dissipated by photoevaporation. This process is caused by photons in the EUV regime, with energy $h\nu > 13.6$ eV, and even more energetic X-ray photons that ionize the gas in the circumstellar disks, raising the disk temperature to more than 10^4 K; and photons in the far ultraviolet (FUV) regime, with energy between $6\,\mathrm{eV} < h\nu < 13.6\,\mathrm{eV}$, that dissociate the gas molecules, heating the gas in the disk up to few 10^3 K. At these temperatures, the high thermal pressure in the disk drives a flow of gas away from its surface, depleting the disk of both gas and small dust grains (Johnstone et al. 1998; Balog et al. 2006).

In the Trapezium in Orion, the externally induced photoevaporation is mainly driven by the FUV radiation, given that the EUV radiation is easily absorbed by the intervening material and the photoevaporative gas itself. In the latter case, the incident EUV radiation ionizes the outflowing gas at a distance from the disk surface, called the "*ionization radius*" (r_{if}), which depends on several variables, such as the intensity of the incident UV flux. This ionized outflowing gas forms an envelope with a characteristic cometary shape with a head pointed toward the ionizing source and molded by the incident radiation and stellar wind (Johnstone et al. 1998; Störzer & Hollenbach 1999). The evaporating protoplanetary disks (*proplyds*) observed in

the Trapezium by the *HST* are at distances $\leqslant$0.5 pc from Θ^1 Ori (Henney & O'Dell 1999). However, consequences of externally induced photoevaporation have been observed at larger distances in other clusters hosting more massive stars, such as in NGC 2244 (Balog et al. 2007), NGC 6611 (Guarcello et al. 2007, 2009, 2010), Pismis 24 (Fang et al. 2012), and Cygnus OB2 (M. G. Guarcello 2014, in preparation).

Candidate evaporating proplyds also have been observed in other clusters: in NGC 2244, IC 1396, and NGC 2264 (Balog et al. 2006); W5 (Koenig et al. 2008); the Trifid Nebula (Yusef-Zadeh et al. 2005); the Lagoon Nebula (Stecklum et al. 1998); the Carina star-forming region (Smith et al. 2003); NGC 3603 (Brandner et al. 2000); and Cygnus OB2 (Wright et al. 2012, 2014). The latter two groups are the best candidates for being actual evaporating proplyds rather than EGGs. In the young and massive association Cygnus OB2 (Wright et al. 2010), the 10 proplyd-like objects were discovered by Wright et al. (2012) analyzing Hα images of this area obtained from the Isaac Newton Telescope (INT) Photometric H-Alpha Survey (IPHAS, Drew et al. 2005). These objects are found at distances between 6 pc and 14 pc from the main group of O stars of the association. The size of their envelopes range from 18×10^3 to 113×10^3 AU, which is much larger than those observed in Orion (40–400 AU; Henney & O'Dell 1999). Wright et al. (2012) suggested a classification of these objects as photoevaporating protostars, mainly given the presence of a central protostar in 70% of the cases, some of which are classified as embedded stars with disks by Guarcello et al. (2013).

In this paper, we study optical low-resolution spectra of the central protostar in the proplyd-like objects #5 and #7, using the nomenclature of Wright et al. (2012), to probe their nature and physical conditions and confirm their classification as stars with evaporating disks. The paper is organized as follows. The properties of the two objects are described in Section 2 and data reduction is described in Section 3. In Section 4, we classify the two central stars and study their circumstellar environments. The accretion, outflow, and variability are studied and discussed in Sections 5, 6 and 7.

2. THE TARGETS

Figure 1 shows two composite images in Hα (green), 8.0 μm (red), and *r* band (blue) of the two targets of this study. The Hα data are taken from IPHAS, those at 8.0 μm from the *Spitzer Legacy Survey of the Cygnus X region* (Beerer et al. 2010), those in the *r* band from IPHAS (upper panel) and observations from the Optical System for Imaging and low-Resolution Integrated Spectroscopy (OSIRIS) mounted on the 10 m Gran Telescopio Canaria (GTC; Cepa et al. 2000), shown in the bottom panel (see Guarcello et al. 2012 for the analysis of the OSIRIS data of Cygnus OB2). In both images, the position of the central star is marked with a circle. In this paper, we assume a distance from the Sun of both objects of 1400 pc (Rygl et al. 2012).

2.1. Protostar #5

The envelope surrounding protostar #5 (α = 20:33:11.66, δ = 40:41:54.3) has a length of 75×10^3 AU and a projected distance of 13.9 pc from the central cluster of O stars (Wright et al. 2012). The central star has been identified by Comerón et al. (2002) as a candidate OB star based on NIR photometry and low-resolution spectroscopy. This object lies outside the field of the Chandra Cygnus OB2 Legacy Project (J. J. Drake 2014, in preparation) and thus it is not included in the list of stars with

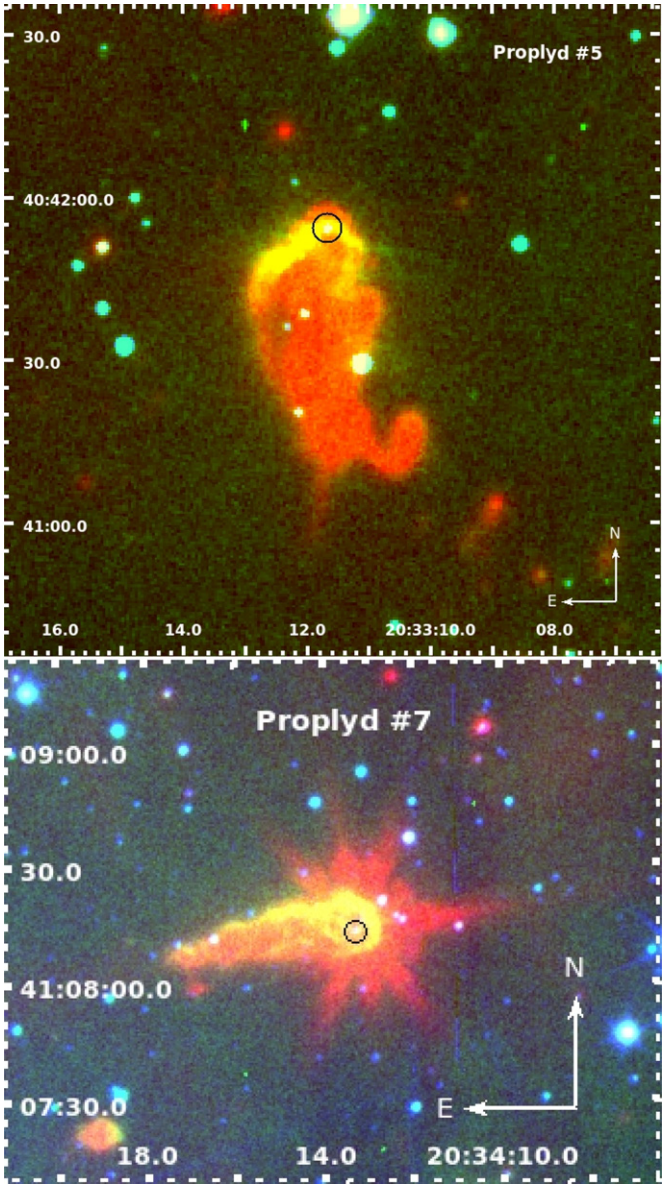

Figure 1. RGB images of the area surrounding protostars #5 (upper panel) and #7 (bottom panel). In both images, the emission at 8.0 μm from *Spitzer* is red, Hα (from IPHAS) is green, and *r* band is blue (from IPHAS in the upper panel and from OSIRIS in the bottom panel). The circles mark the position of the candidate embedded star observed with OSIRIS and IPHAS.

(A color version of this figure is available in the online journal.)

disks in Cygnus OB2 compiled by Guarcello et al. (2013). Its photometry (from the SDSS Data Release 9, IPHAS, UKIDSS public catalog, and IRAC from the Spitzer Legacy Survey of the Cygnus X region) is shown in Table 1. It is a bright infrared source with colors in Spitzer bands typical of an embedded star with a circumstellar disk (M. G. Gutermuth et al. 2008; Guarcello et al. 2013).

The position of the embedded young stellar object (YSO) corresponds to the ionization front in the envelope, although this may be a projection effect. This object is expected to be irradiated by a FUV flux of 1436 G_0[8] and an EUV flux of 3.9×10^{10} photons s^{-1}. These fluxes are calculated by projecting

[8] In terms of the Habing flux "G_0," equal to 1.6×10^{-3} erg cm^{-2} s^{-1}; $G_0 = 1.7$ corresponds to the average UV flux in the 912–2000 Å spectral range in the Solar neighborhood (Habing 1968).

Table 1
Photometry of the Central Star in Protostar #5

SDSS				
u (mag)	*g* (mag)	*r* (mag)	*i* (mag)	*z* (mag)
24 ± 1	23.7 ± 0.9	19.8 ± 0.4	18.0 ± 0.3	16.4 ± 0.2
IPHAS				
r (mag)		*i* (mag)		Hα (mag)
19.7 ± 0.02		17.47 ± 0.02		18.07 ± 0.02
UKIDSS				
J (mag)		*H* (mag)		*K* (mag)
13.395 ± 0.001		11.894 ± 0.001		15.513 ± 0.001
Spitzer				
[3.6] (mag)	[4.5] (mag)	[5.8] (mag)	[8.0] (mag)	
8.648 ± 0.007	7.824 ± 0.004	7.078 ± 0.002	6.16 ± 0.04	

and summing the expected FUV and EUV fluxes emitted by each O star in Cyg OB2 at the position of object #5 using the intrinsic UV fluxes for O stars tabulated in Parravano et al. (2003) and Martins et al. (2005) and their known spectral types (Wright 2014). These fluxes are upper limits considering that we used the projected distances from the O stars and we ignored the intracluster absorption. For comparison, similar fluxes are experienced at distances of 1.3–1.4 pc from an O6V star such as Θ^1 Ori.

Protostar #5 has been identified by Griffith et al. (1991) as a 5 GHz continuum source. It has been named "the Cradle Nebula" by Strelnitski et al. (2013), who identified it as a strong compact source in ^{12}CO maps, and as a bright object in *Spitzer* and *Herschel* images, with different morphology at different wavelengths. In particular, the envelope presents a secondary clump on the western side that does not appear to be hosting a T Tauri star.

2.2. Protostar #7

Protostar #7 is located at α = 20:34:13.27, δ = 41:08:13.8, at a projected distance to the center of the association of 5.6 pc and with an envelope with an elongated structure 77 × 10^3 AU long (Wright et al. 2012). This object, also known as IRAS 20324+4057, was observed by the *HST* (PI: Sahai) with the Advanced Camera for Surveys using broadband filters F606W (λ_c = 5907 Å) and F814W (λ_c = 8333 Å). A composite image of these two bands is shown in Wright et al. (2012).

A study by Pereira & Miranda (2007) concluded that the envelope is a photoionized region rather than a shock-excited nebulosity. The central star has been classified by Comerón et al. (2002) as a young massive star. In the bottom panel in Figure 1, the central star is clearly detected using OSIRIS by Guarcello et al. (2013) in their search for the members of Cyg OB2 with disks. The central star is number 1724 in their list of stars with disks and it has been classified as a class I object. Its optical counterpart is faint ($r = 22.65^m \pm 0.03^m$), while the infrared counterpart is bright and red ($[3.6] = 5.330^m \pm 0.002^m$, $[3.6]-[4.5] = 1.019^m \pm 0.004^m$).

The envelope surrounding protostar #7 has a canonical teardrop shape, with the embedded YSO at a distance of ∼5″ from the ionization front (about 7000 AU). This object is estimated to be irradiated by a FUV flux of 2802 G_0 and an EUV flux of 8.8 × 10^{10} photons cm^{-2} s^{-1}, enough to induce the photoevaporation of the circumstellar disk (M. G. Guarcello 2014, in preparation).[9] An O6V star like Θ^1Ori produces a similar flux at a distance of 0.9 pc, similar to the distance from Θ^1 Ori at which the evaporating proplyds in the Trapezium in Orion are observed.

3. OBSERVATIONS AND DATA REDUCTION

The two targets were observed with OSIRIS@GTC with a granted observing time of 4 hr (proposal GTC 28-12B). The log of the observations is shown in Table 2. Observations were obtained on two different nights (2012 August 10, OB2, and 2012 August 14, OB4), both with good seeing conditions. Protostar #5 was observed using three different grisms: R1000B (three exposures of 180 s each), R2500R and R2500I (one 870 s exposure with each grism); protostar #7 was observed six times using the R1000R grism, with exposures of 870 s. We used slits with a width of 1.″2 and the spectra were taken with 2 × 2 binned pixels, as in the standard operation mode. Table 3 lists the central wavelengths and spectral ranges of the grism we used. On each night of observation, arc lamp spectra, flat-field images, biases and spectra of spectrophotometric standards were taken.

We reduced the spectra using standard IRAF routines.[10] Spectra and calibration images were corrected for overscan, bias, and flat field using *CCDPROC*. The bias images were combined using average and *minmax* rejection. We produced a master flat for each night by combining all the flat images available with the task *RESPONSE*. The final wavelength and flux calibration was done using *DOSLIT*. Given the highly variable diffuse emission around each target, no background subtraction was attempted.

The GTC/OSIRIS spectra analyzed in this work are shown in Figure 2, in which multiple spectra taken with the same grism are combined. The blue part (λ < 5000 Å) of the R1000B spectrum of protostar #5 is not shown here since it is completely dominated by noise. The atmospheric absorption features that in some cases dominate the spectra, such as at ∼7600 Å and ∼9500 Å, are also marked. Several emission lines, mainly from protostar #7, are evident. They provide excellent diagnostics for the infall/outflow process and the circumstellar environment and they will be analyzed in the next sections. Equivalent widths (EW) and line fluxes were measured using the IRAF task *SPLOT*. The spectra of both objects have been corrected for extinction using the IRAF task *DEREDDEN* before measuring the line equivalent width and flux. We extracted a region of ∼60 Å around the line and then normalized the extracted dereddened spectrum to the continuum using the task *CONTINUUM*. EW and line fluxes were derived by fitting the line with a Voigt profile if $EW \geqslant 100$ mÅ or with a Gaussian if $EW < 100$ mÅ.

4. PROPERTIES OF THE CENTRAL PROTOSTAR

4.1. Spectral Classification

As discussed in Section 2, the two protostars were classified as embedded OB stars by Comerón et al. (2002) after analyzing

[9] As shown by Johnstone et al. (1998), the disks of the proplyds in Orion are mainly irradiated by the FUV radiation. The EUV photons are in fact absorbed by the photoevaporating gas and the surrounding envelope, while copious FUV photons reach the disk. In this object, a bright ionization front is evident in the part of the envelope facing the O stars, so in principle, the same process may be in action.

[10] IRAF is distributed by the National Optical Astronomy Observatory, which is operated by the Association of Universities for Research in Astronomy (AURA) under cooperative agreement with the National Science Foundation.

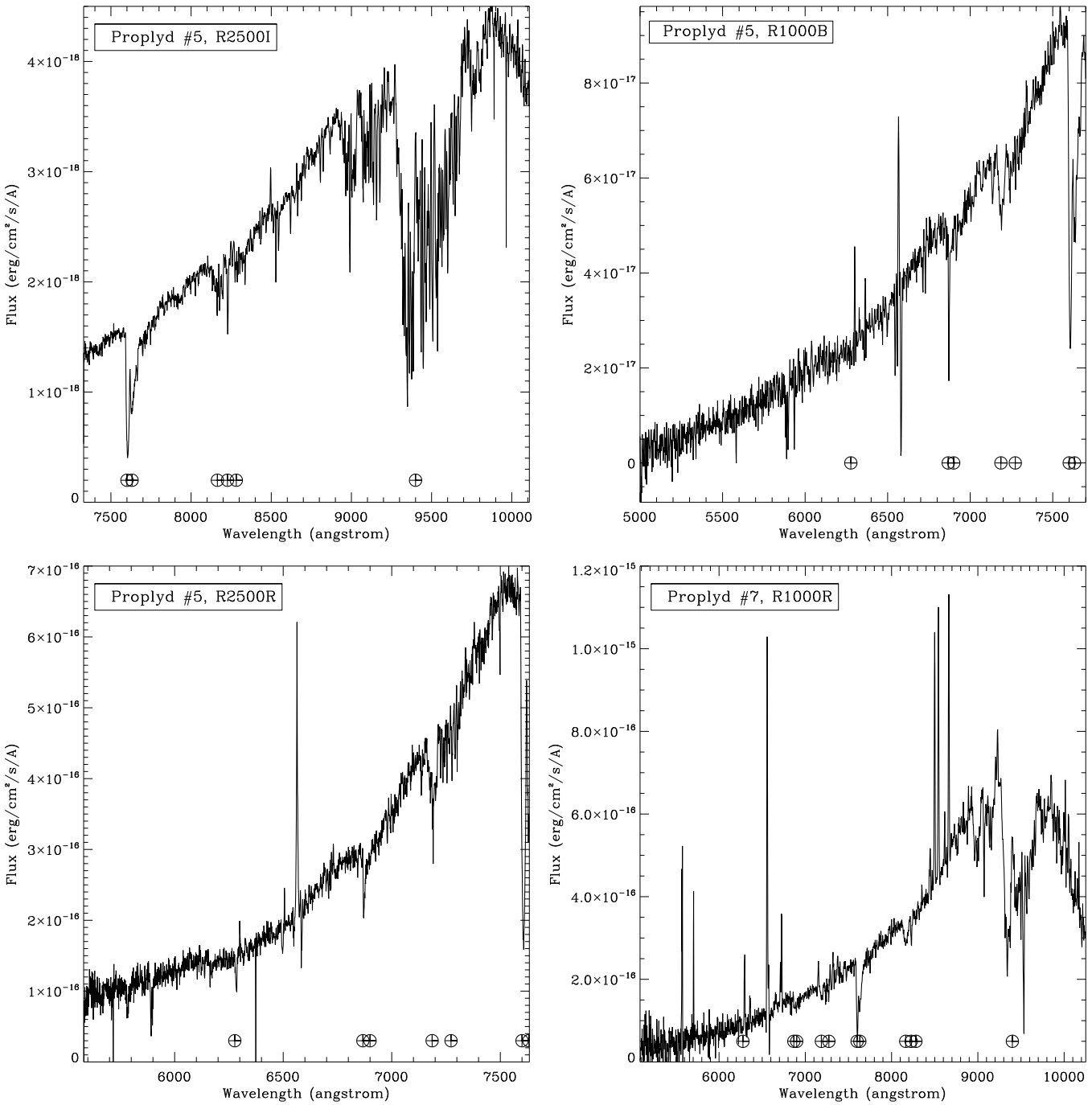

Figure 2. Reduced and calibrated, but not corrected for the extinction, spectra of protostars #5 (upper and lower left panels) and #7 (lower right panel). The grism used and the telluric absorption features are also indicated.

Table 2
Log of the Observations

OB	Target	Date	Grism	Seeing	Exposure Time	Standard
OB1	protostar #5	2012 Aug 10	R1000B	$\leqslant 1\farcs25$	3×180 s	L1363-3
OB2	protostar #7	2012 Aug 10	R1000R	$\leqslant 1\farcs16$	2×870 s	L1363-3
OB3	protostar #5	2012 Aug 14	R2500R, R2500I	$\leqslant 1\farcs09$	2×870 s	G158-100
OB4	protostar #7	2012 Aug 14	R1000R	$\leqslant 1\farcs31$	4×870 s	G158-100

their infrared spectra. We attempted a spectral classification for these two stars using the atlases compiled by Walborn & Fitzpatrick (1990) and Torres-Dodgen & Weaver (1993), the classification of spectral standards by Allen & Strom (1995) and the *SPTclass* code which uses the spectral classification scheme optimized for Herbig Ae/Be stars of Hernández et al. (2004).

The spectrum of protostar #7 does not show TiO bands or the Paschen series typical of KM and OBAF stars, respectively. For this reason, a spectral classification as a G star is more likely.

Table 3
Width and Central Wavelength of the Used Grisms

Grism	λ_c (Å)	Spectral Range (Å)
R1000R	7510	5100–10000
R1000B	5510	3630–7500
R2500R	6590	5575–7685
R2500I	8740	7330–10000

However, the spectra of protostar #7 do not show any particular absorption features typical of G stars, such as the Na I λ5893 absorption line. This classification is thus still preliminary. We also compared the optical–infrared spectral energy distribution (SED) of protostar #7 with the grid of YSOs SED provided by Robitaille et al. (2007). The observed SED fits models of both early and late stars, affected by an interstellar extinction ranging from $A_V \sim 9^m$ to $A_V \sim 12^m$. All the fitting models agree with an age younger than 1 Myr. Using the 1 Myr isochrone from Siess et al. (2000) and adopting the distance of 1400 pc, an extinction of about $A_V = 12^m$ can be compatible with a G star, while smaller extinctions would be more compatible with later stars that we discard for the lack of observed TiO bands in the spectra. In the following, we adopt a G spectral type and we use an extinction of $A_V = 12^m$ to deredden the spectra. However, we will show that our results are not qualitatively affected by adopting different values of extinction and stellar parameters.

The lack of absorption lines can be a consequence of veiling due to intense accretion from the disk. The accretion flow originates from the inner boundary of the disk, where the magnetic field funnels the gas that accretes onto the stellar surface (Uchida & Shibata 1984). The accreting material falls at velocities of few hundred km s^{-1}, forming accretion spots at the footpoints of the open magnetic funnels. The energy released by the accretion process heats the accretion spots up to few 10^4 K. In this way, both the accreting material and the plasma in the accretion spots become sources of optical, UV, and soft X-ray radiation. This optical continuum emission, added to the photospheric emission, fills the photospheric absorption lines that consequently become weaker (e.g., Calvet & Gullbring 1998). We will demonstrate that protostar #7 is actively accreting and the consequent veiling of its optical spectrum is a natural explanation for the lack of absorption lines.

Several absorption lines are observed instead in the spectra of protostar #5 (see Figure 3). The lack of Paschen lines in absorption excludes a spectral type earlier than G, while the lack of TiO bands excludes a spectral class later than late K (Torres-Dodgen & Weaver 1993). A G–early K spectral type is then the most likely solution. This is also supported by the presence of other absorption features such as several Fe I lines between 7700 Å and 8900 Å, the Be II+Fe I+Ca I blend at 6497 Å, and the Mg I λ8807 line. Furthermore, the EW of Na I λ5893 is 5.8 ± 0.5 Å, which is typical of K2–K4 stars as indicated by SPTclass, and the EW of Fe I λ6495 is 1.45 ± 0.05 Å, indicating a spectral class earlier than K5. Merging these results, we adopt a spectral class of K2 ± 1 for protostar #5, which corresponds to a mass larger than 2.2 $M_\odot$ for stars younger than 1 Myr (Siess et al. 2000). Figure 3 shows the lines that we used for the spectral classification of this star.

4.2. Evidence of Youth

A Li λ6708 absorption line with an EW ∼ 0.46 Å is present in the spectra of protostar #5 (see Figure 4). This line is usually adopted as a criterion for selecting young stars. Lithium is burned at relatively low temperatures ($2.5–3.0 \times 10^6$ K) and convective mixing can rapidly bring the lithium from the photosphere to the stellar interior. As a consequence, Li is rapidly consumed during the pre-main-sequence (PMS) phase and its presence can be used as a diagnostic for stellar youth (Randich et al. 2005). However, the efficiency of Li depletion varies markedly with stellar mass. In stars more massive than 1 $M_\odot$, a radiative core develops during the contraction toward the main sequence before the Li depletion is complete, reducing the efficiency of the convective mixing and resulting in longer Li depletion timescales. In Section 4.1, we classified protostar #5 as a K2 ± 1 star, with $M_\star \geqslant 2.2\,M_\odot$. In this mass range, a timescale for Li depletion longer than 10 Myr can be expected (Jeffries & Oliveira 2005). It is not surprising, then, that we observe a Li λ6708 absorption line in protostar #5.

The best clue for the young age of both protostars is provided by the presence of circumstellar disks which are actively accreting, as well as the presence of outflow. In young clusters the fraction of members still bearing a disk is observed to decline from about 80% in clusters younger than 1 Myr, to ∼55% at 3 Myr and ∼15% at ∼5 Myr (Haisch et al. 2001; Hernández et al. 2007; Mamajek 2009), indicating a rapid dissipation of disks. The timescale for disk dissipation is even faster in stars as massive as protostars #5 and #7 (e.g., Lada et al. 2006). The presence of a circumstellar disk, found by Guarcello et al. (2013) for protostar #7 and by the present work for protostar #5, then allows us to conclude that the central stars in these two proplyd-like objects are at most just a few Myrs old. Additionally, as we will show later, the spectra of both protostars show signatures of infall/outflow. The accretion process is expected to decline faster than the typical timescales for disk dissipation (Fedele et al. 2010). In conclusion, all the evidence points toward an age for these two objects ranging from a few 10^5 yr to ∼2 Myr.

4.3. The Circumstellar Environment of Protostar #7

One of the aims of our study is to understand whether the circumstellar disks around these two protostars are photoevaporating under the influence of the incident UV radiation. One clue in this sense is provided in the spectrum of protostar #7 by the presence of the O I λ8446 emission line (Figure 5). This line is produced primarily through the $Ly\beta$ fluorescence process (Bowen & Swings 1947), in which the O I 3d ^{3}D state is photoexcited upon absorption of $Ly\beta$ photons by the ground state, and then it decays with emission at 11287 Å, 8446 Å, and 1304 Å in succession. This process was called *photoexcitation by accidental resonance* (PAR) by Kastner & Bhatia (1995), who constructed a detailed model for neutral oxygen and computed expected strengths of the various O I lines (also accounting for collisional excitation). The O I λ8446 emission line has been observed in environments characterized by intense local UV fields, such as the star forming regions in the Orion Nebula (Münch & Taylor 1974; Grandi 1975) and the circumstellar environment of η Carinae (Johansson & Letokhov 2005), in Be stars (Mathew et al. 2012), and in extragalactic objects such as Seyfert galaxies (Grandi 1980). There is no diagnostic that allows us to connect the flux observed at O I λ8446 with the intensity of the local $Ly\beta$ flux, but its presence in the spectrum indicates that the emitting gas is irradiated by UV photons. This UV flux can originate from the massive members of the association, if the intracluster extinction is not severe, or it can be produced by intense accretion, as discussed in Section 4.1.

The intense UV flux is expected to increase the level of ionization in the circumstellar gas. Evidence for the presence of a large

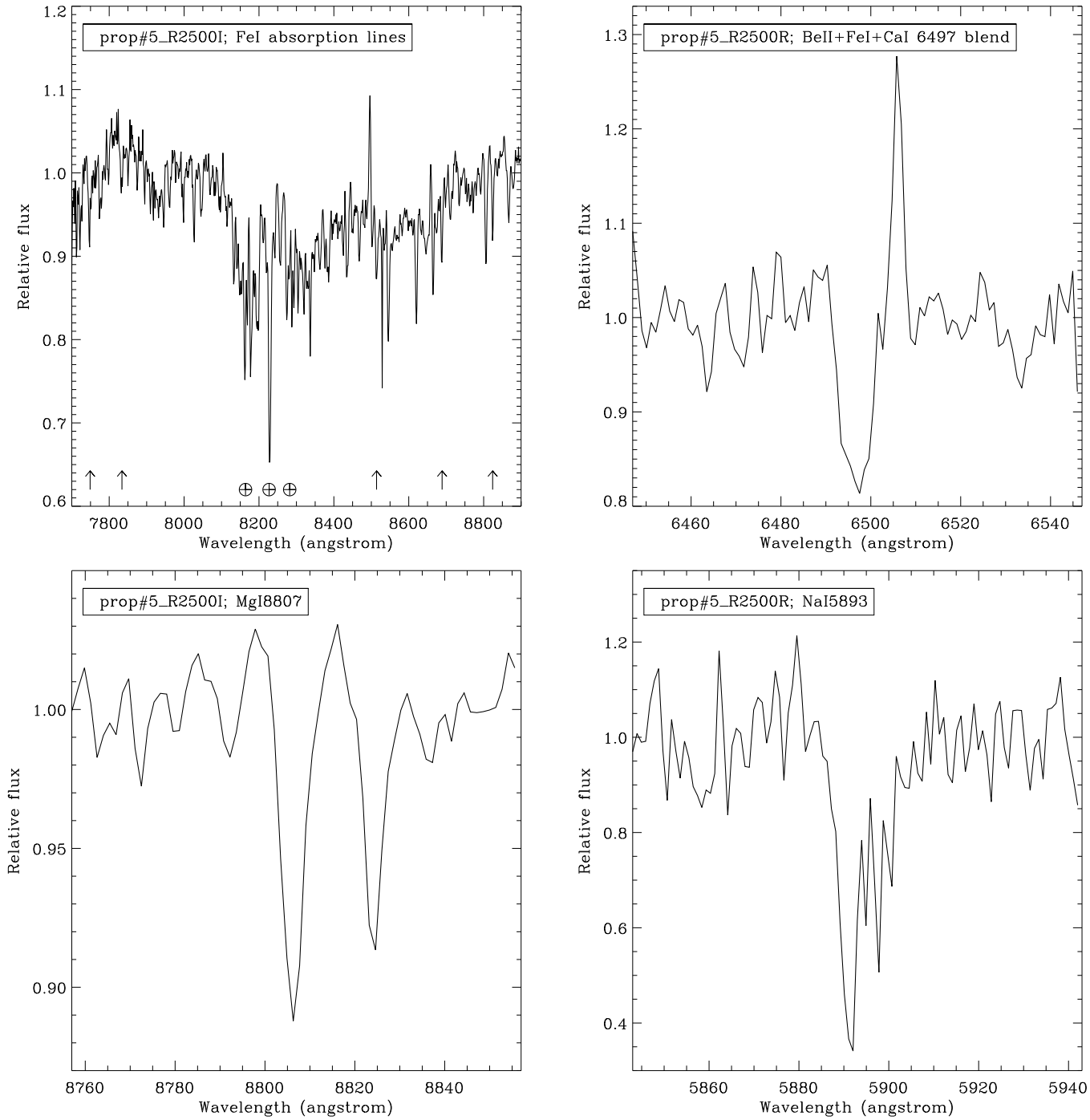

Figure 3. Lines used for the spectral classification of protostar #5. The complex of Fe I absorption lines (marked with upward arrows), the Be II+Fe I+Ca I λ6497 blend, the Mg I λ8807 line, and the Na I λ5893 line. All the spectra are normalized on the continuum.

amount of ionized gas in the circumstellar environment of protostar #7 is provided by the low [O I] λ6300/([S II] λ6716 + [S II] λ6731) observed ratio. These lines will be discussed in detail later in this paper and used as diagnostics for electron density and mass loss rate. In this section, we compare the ratio of their fluxes with the values typically observed in other T Tauri stars. In their analysis of the optical spectra of 42 T Tauri stars, Hartigan et al. (1995) found a typical [O I] λ6300/([S II] λ6716 + [S II] λ6731) ratio ranging between 2 and 4, with no stars with a ratio smaller than 1.5. It must be noted that these 42 T Tauri stars are members of regions where no intense ionizing radiation field is expected, such as the Taurus Molecular Cloud. In the combined spectra of protostar #7, adopting an extinction $A_V = 12^m$, the ratio is 1.38 (1.25 only in the OB4 spectra, where all the three lines are intense, while in the OB2 it was not possible to calculate this ratio), which is lower than what observed by Hartigan et al. (1995). Ratios similar to what we find in protostar #7 have been found in the proplyds in Orion (Bally et al. 1998; Henney & O'Dell 1999) and in the candidate photoevaporating star SO587 in σ Orionis (Rigliaco et al. 2009).

The presence of the O I λ8446 emission line and the atypical [O I] λ6300/([S II] λ6716 + [S II] λ6731) ratio indicate that the circumstellar environment of protostar #7 is irradiated by an intense local UV field and that the fraction of ionized gas is

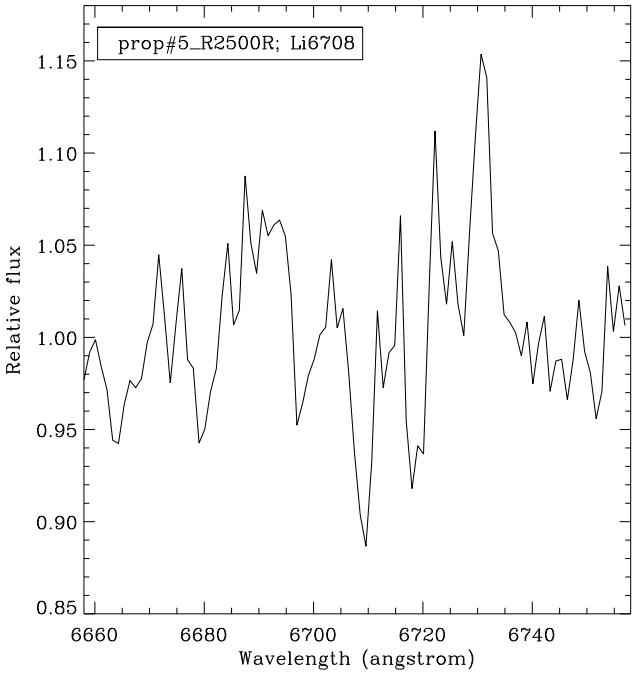

Figure 4. R2500R spectrum of protostar #5 around the faint absorption feature that may correspond to the Li λ6708 absorption line (in the center).

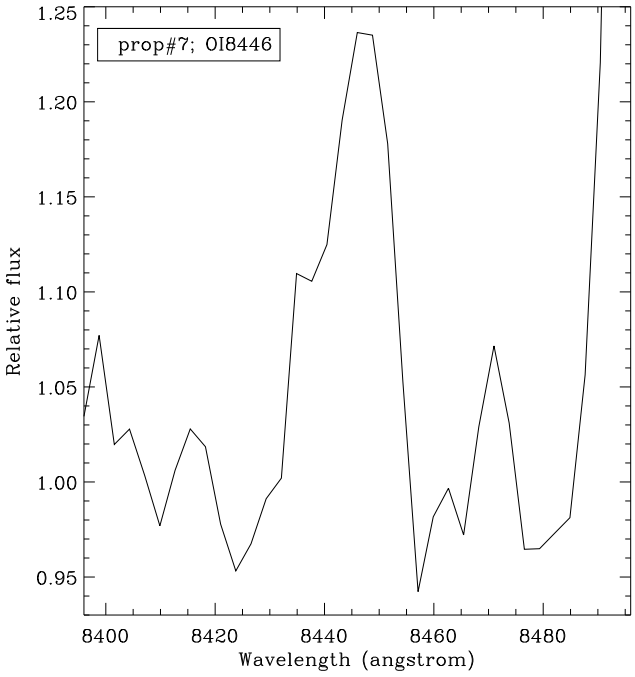

Figure 5. O I λ8446 emission line of protostar #7. The blue part of the Ca I λ8498 emission line is also evident.

larger than typically observed in T Tauri stars, but similar to what is observed in photoevaporating disks.

5. ACCRETION AND OUTFLOW

In this section, we study the accretion and the outflow in protostar #7 using several emission lines. None of these, with the exception of Hα, are observed in the spectra of protostar #5.

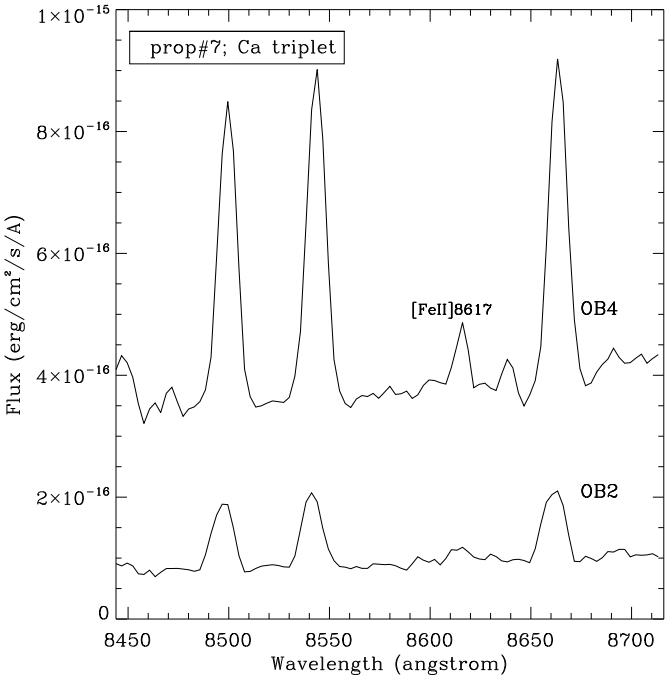

Figure 6. Region of the spectrum of protostar #7 containing the infrared Ca II triplet and the [Fe II] λ8617 emission line, observed in OB2 (fainter spectrum) and OB4 (brighter spectrum). The offset between the two spectra is due to the variability of this source.

5.1. Accretion Rate and Luminosity

Both stars show signatures of active accretion, which is common in very young T Tauri stars with disks. Typically the mass accretion rate observed in T Tauri stars declines with the age of the disk (e.g., Hartmann et al. 1998) and it varies with the mass of the central star with an empirical scaling law $\dot{M} \propto M_{\star}^{2}$ (Alexander & Armitage 2006). One common signature for active accretion is the presence in the spectra of the 8498 Å, 8542 Å, and 8662 Å Ca II triplet lines (Herbig & Soderblom 1980; Muzerolle et al. 1998), which can be easily excited by the veiling continuum produced in the accretion spots. Several clues suggest that the Ca II triplet is emitted by gas in the inner boundary of circumstellar disks and in the accretion flow (Kwan & Fischer 2011).

The red part (i.e., $\lambda \geqslant 8400$ Å) of the protostar #7 spectrum is dominated by an intense Ca II triplet (see Figure 6). The intensity ratio between the three lines provides clues about their nature; if emitted by optically thin material, their ratio is given by the ratio of their gf values, 1:9:5 for 8498:8542:8662 Å, respectively (Wiese et al. 1969); while if emitted by optically thick gas, the lines saturate and the ratio flattens out. The ratio we observe in the combined spectrum of protostar #7 is 1:1.1:1, with slight differences between the OB2 and OB4 spectra. This ratio indicates that the Ca II triplet is emitted by optically thick material, as typically observed in accreting T Tauri stars.

A correlation between the intensity of the Ca II λ8542 line and the accretion luminosity was found by Muzerolle et al. (1998) and Calvet et al. (2000):

$$\log(L_{\rm acc}/L_{\odot}) = (0.85 \pm 0.12)\log(L_{8542}/L_{\odot}) + (2.46 \pm 0.46). \quad (1)$$

After the reddening correction (with $A_V = 12^m$), the flux emitted in the Ca II λ8542 line by protostar #7 is 4.72×10^{-13} erg cm^{-2} s^{-1} Å in the OB2 spectrum and

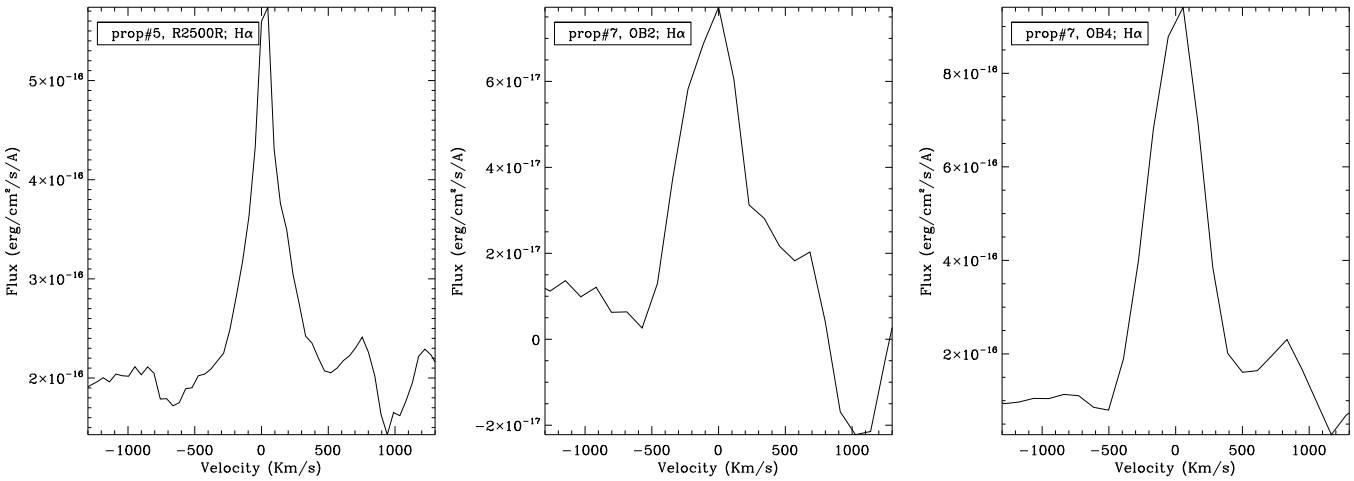

Figure 7. Hα emission line observed in the R2500R spectrum of protostar #5 and the spectra of protostar #7 in two OBs, with the redshifted and blueshifted (at about $\pm$500 km s^{-1}) absorption features.

1.98×10^{-12} erg cm^{-2} s^{-1} Å in OB4. Converting these values into luminosity and using Equation (1), these fluxes correspond to $L_{\rm acc} = 5.45 \times 10^{34}$ erg s^{-1} (OB2) and $L_{\rm acc} = 1.84 \times 10^{35}$ erg s^{-1} (OB4). This difference in flux observed in the two OBs for the Ca II λ8542, as well as other in other lines as described later, is intrinsic given that the spectra have been flux-calibrated (Section 3).

To convert $L_{\rm acc}$ into mass accretion rate, we use the equation defined by Gullbring et al. (1998):

$$\dot{M} = \frac{L_{\rm acc} R_\star}{G M_\star} \left(1 - \frac{R_\star}{R_{\rm inner}}\right)^{-1}. \quad (2)$$

Since the spectral classification of protostar #7 is not accurate, we consider a range of possible spectral classes, and we calculate the corresponding $\dot{M}$ using Equation (2) and the stellar parameters in this range from the 0.5 Myr isochrone of Siess et al. (2000): we adopted $4\,M_\odot < M_\star < 5\,M_\odot$ and $8\,R_\odot < R_\star < 10.4\,R_\odot$. Using these values, the accretion rate ranges between $1.13 - 1.17 \times 10^{-6}$ $M_\odot$ yr^{-1} for OB2, and $3.8–4.0 \times 10^{-6}$ $M_\odot$ yr^{-1} for OB4.

Another line usually observed in accreting T Tauri stars that can be used as a diagnostic of mass accretion rate is the Hα line. For instance, Natta et al. (2004) correlated the Hα 10% width with the accretion rates observed in a sample of 19 very low mass objects in Chamaleon I and ρ Ophiuchi. The use of the width at 10% of the peak is meant to reduce the sensitivity to contamination from the nebula emission around the star, which is not always trivial to remove. In these two objects, the nebula contribution is very intense and it arises from the intense emission in Hα from the envelope (Wright et al. 2012), so we have not attempted this estimate. Figure 7 shows the Hα profile observed in the R2500R spectrum of protostar #5 and that in protostar #7 observed in the two OBs. In all the profiles, the base of the line is broad, as expected in accreting objects, with the narrow peak due to nebular emission being more evident in #5. Other features include the evident absorption at $\pm$500 km s^{-1} (more evident in #5). Redshifted absorption features at velocities exceeding 100 km s^{-1} are a signature of accretion (Appenzeller & Wolf 1977; Edwards et al. 1994), while blueshifted absorption, more rarely observed in T Tauri stars, indicates the presence of outflows (Hartigan et al. 1995). The Hα profiles in the two targets, then, even if not useful to quantify the mass accretion rate, provide evidence for presence of infall and outflow in both objects.

Another clue about the presence of intense accretion in protostar #5 is provided by the IPHAS colors. Using the IPHAS colors of normal stars derived by Drew et al. (2005), a K2 $\pm$1 star with r-in $= 2.2^m$ is supposed to have $r - {\rm H}_{\rm alpha} = 0.66^m$, while this protostar has $r - {\rm H}\alpha = 1.63^m$. This is significantly larger than the color expected for normal stars, and compatible with an intense Hα emission due to accretion (Barentsen et al. 2011), although some level of contamination of the Hα photometry of this object may be present.

5.2. Outflow

Classical T Tauri stars often show signatures of outflow. The presence of a slow and wide wind driven off from the circumstellar disk is used to explain both the blueshifted forbidden emission lines and redshifted absorption features that are associated with the emission lines, which are typically observed in T Tauri stars, with the hypothesis that the disk obscures the part of the wind that is moving away from the observer. The presence of high-velocity collimated jets has also been proved by direct high-resolution imaging observations of T Tauri stars such as DG Tau and HL Tau (i.e., Solf 1989), and the presence of blueshifted high-velocity components in the emission lines (Hartigan et al. 1995). There is a growing body of evidence that these outflows are powered by the accretion in the disk and a correlation between the mass loss rate and mass accretion rate is observed, with the former usually being two orders of magnitude less than the latter (Cabrit et al. 1990).

In the spectra of protostar #7, several forbidden emission lines (FELs) are observed. FELs, such as [O I] λ6300 or the [S II] λ6731+6716 doublet, are observed from a variety of low-density astrophysical environments, where the decay of electrons from meta-stable states is more likely to occur spontaneously rather than after collisions. In young stellar objects, they usually serve as powerful tracers and diagnostics for outflow activity close to star and disk (Hirth 1994). Figure 8 shows the main FELs observed in the spectra of protostar #7. The upper panel shows the [S II] doublet, used as a diagnostic for electron density. We observe a significant variation of both the shape and the intensity of this doublet among the two OBs. In OB2 it is almost undetected, with an absorption feature that may not be real; in OB4, the two lines of the doublet are evident and easily

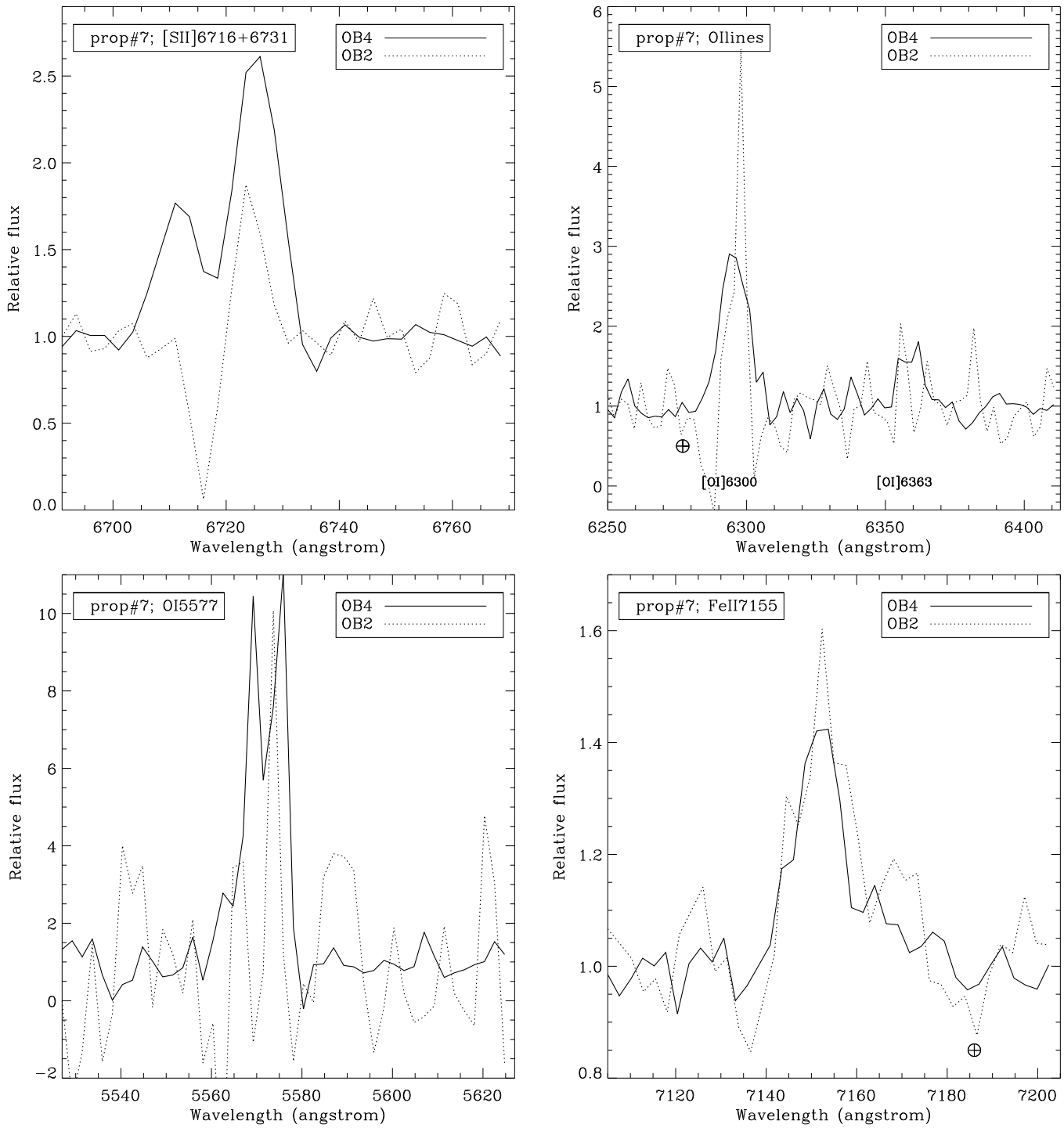

Figure 8. Forbidden emission lines observed in the spectra of protostar #7. In all the panels, the solid lines mark the spectrum taken during OB4 and the dotted lines mark the spectrum taken during OB2. The panels show [S II] λ6716+ λ6731 doublet (upper left), [O I] λ6300 and [O I] λ6363 lines (upper right), [O I] λ5577 line (lower left), and [Fe II] λ7155 line (lower right). The positions of telluric absorption features are also indicated.

distinguishable. The second panel shows the region of the spectra containing the [O I] λ6300 and [O I] λ6363 lines. The former is present in both spectra with an asymmetric shape that will be discussed later; the latter is present only in the OB4 spectrum. The third panel shows the [O I] λ5577 line. The OB2 spectrum is very noisy and it is not clear whether the line is present or not, while in OB4 the line is more evident. Finally, the fourth panel shows the [Fe II] λ7155 line, which is present and asymmetric in both spectra. The [Fe II] FEL at 8617Å is observed and shown in Figure 6.

5.3. Profiles of the FELs

The centroid of the FELs observed in T Tauri stars is always blueshifted. This is an indication that the source of the emission is not the star itself, but outflowing material in the wind and/or a jet (Cabrit et al. 1990). Another important feature of the FELs is that they are often multi-component (i.e., Hartigan et al. 1995; Hirth et al. 1997; Whelan et al. 2004), with a superposition of a low-velocity (typically few km s^{-1}) and a high-velocity (typically a few hundreds km s^{-1}) component (LVC and HVC,

Table 4
Centroid Velocity of the Observed FELs

Line	OB2 Velocity ($km\,s^{-1}$)	OB4 Velocity ($km\,s^{-1}$)
[O I] 5577	-174 ± 12	-62 ± 3
[O I] 6300	-47 ± 8	-210 ± 9
[O I] 6363	NAN	-65 ± 15
[S II] 6716	NAN	-178 ± 20
[S II] 6731	-307 ± 16	-249 ± 14
[Fe II] 7155	-102 ± 41	-130 ± 73
[Fe II] 8617	NAN	-31 ± 7

respectively). Strong evidence exists that the HVC observed in FELs is emitted by stellar jets, such as images at high spatial resolution where it is possible to resolve the region where the line is actually produced (i.e., Kepner et al. 1993; Whelan et al. 2004), while the LVC is emitted by a broad and slow disk wind (Kwan & Tademaru 1988; Kwan 1997).

The FELs observed in protostar #7 are blueshifted as reported in Table 4 and the two velocity components can be distinguished only in few lines, given the low resolution of our spectra. In the few cases where two peaks are present, Table 4 lists the centroid velocities of the low velocity component. The velocities are larger than the values typically observed in T Tauri stars (i.e., Cabrit et al. 1990), but examples of stars with such high-speed outflows are present in the literature (i.e., DG Tau and LkHα 321, Whelan et al. 2004).

The centroids of the FELs were measured fitting the line profile as explained in Section 3 using *SPLOT*. Given that the results of the fit change slightly when adopting different starting points across the line profile, we repeated the fit several times for each line changing the starting point each time. The results listed in Table 4 are taken from a median of the measured values. The errors listed are whichever are the larger among the error provided by the line profile fit or the one representing the range in which the nominal value of the centroid varied. We note that our centroid velocities in Table 4 should be interpreted with caution: in the R1000R low-resolution spectra the LVC and HVC are usually not distinguishable and we have no means of determining an accurate correction for the radial velocity of protostar #7.

The only FELs in which the HVC and LVC are distinguishable are the [O I] λ5577 and [O I] λ6363 lines. After deblending the two components of these two lines using *SPLOT*, the LVCs were observed, respectively, at -93 ± 53 km s^{-1} and -150 ± 23 km s^{-1}, while the HVCs were at -296 ± 17 km s^{-1} and -299 ± 27 km s^{-1}, respectively. The presence of FELs, then, demonstrates that protostar #7 is characterized by intense outflow, with marginal evidence also for the presence of a stellar jet.

5.4. Electron Density in the Outflow of Protostar #7

An excellent diagnostic for the electron density is provided by the[S II] λ6716/[S II] λ6731 ratio, which is independent from the temperature of the emitting gas (Czyzak et al. 1986). In T Tauri stars, most of the observed [S II] ratios are close to the saturation value, which occurs at $N_e \geqslant 5 \times 10^3$ cm^{-3} (i.e., Hamann 1994).

The OB4 spectra of protostar #7, shown in Figure 8, have a clear and intense [S II] doublet. In OB2, the [S II] λ6731 line is still evident, but the spectrum is very noisy. To calculate the [S II] λ6716/[S II] λ6731 ratio in the combined OB4 spectrum, we deblended the two lines using *SPLOT* in the dereddened spectra. The best fit is obtained with two Gaussian profiles centered at 6711 Å and 6725 Å, with a flux ratio of 0.47, which is close to the saturated regime (Czyzak et al. 1986). An accurate estimate of the electron density in the outflowing material of protostar #7 can be obtained with the relation found by Proxauf et al. (2014), which gives $\log(N_e) = 4.03$ cm^{-3}. The symmetry of the two lines in the [S II] doublet does not allow us to attribute this electron density to the stellar wind or to an eventual stellar jet, which can be reasonably expected to have different temperature and density (Hartigan et al. 1995). Lacking spatially resolved data for protostar #7 and any evidence for a HVC in these two lines, this electron density will be used as an average value for the whole stellar outflow hereafter.

5.5. Mass Loss Rate in Protostar #7

An intense [O I] λ6300 emission line from protostar #7 was seen in both OBs (see Figure 8). The mass loss rate due to the outflow can be calculated using the equations found by Hartigan et al. (1995):

$$\dot{M} = 2.27 \times 10^{-10} \left(1 + \frac{N_c}{N_e}\right) \left(\frac{L_{[\mathrm{O\,I}]\lambda 6300}}{10^{-4} L_\odot}\right) \times \left(\frac{V_\perp}{150\,\mathrm{km\,s^{-1}}}\right) \left(\frac{l_\perp}{2 \times 10^{15}\,\mathrm{cm}}\right)^{-1} M_\odot\,\mathrm{yr}^{-1}. \quad (3)$$

We adopted the value of 150 km s^{-1} for the outflow velocity $V_\perp$, and 1.97×10^6 cm^{-3} for the critical density N_c, as in Hartigan et al. (1995). We also used the electron density N_e found using the [S II] doublet ratio (Section 5.4) and the slit width $l_\perp$ of 1.″2. We calculated $L_{[\mathrm{O\,I}]\lambda 6300}$ from the line flux observed in the dereddened spectra (adopting $A_V = 12^m$) and adopting the distance of 1400 pc (Rygl et al. 2012). Using the OB4 spectra (from which we have been able to calculate the electron density of the outflow), Equation (3) gives a mass loss rate of 5.0×10^{-5} $M_\odot$ yr^{-1}. In this calculation, we ignored the sky contamination of the [O I] λ6300 emission line. This is justified since the intensity of the sky line is negligible with respect to the intense emission from the protostar.[11] Additionally, the sky line is centered on 6302 Å, while the emission from the protostar is blueshifted and well distinguished from this contamination (see Figure 8 and Section 5.3).

It is also possible to estimate the mass loss rate from the [S II] λ6731 line intensity (Hartigan et al. 1995):

$$\dot{M} = 3.38 \times 10^{-8} \left(\frac{L_{[\mathrm{S\,II}]\lambda 6731}}{10^{-4} L_\odot}\right) \left(\frac{V_\perp}{150\,\mathrm{km\,s^{-1}}}\right) \times \left(\frac{l_\perp}{2 \times 10^{15}\,\mathrm{cm}}\right)^{-1} M_\odot\,\mathrm{yr}^{-1}. \quad (4)$$

Using this equation, we obtain a mass loss rate of 2.2×10^{-5} $M_\odot$ yr^{-1}, similar to the value calculated from Equation (3).

6. VARIABILITY

T Tauri stars are known to be variable sources. For instance, in the Orion Molecular Cloud, 70% of the members with disks and 44% of those with no disks are observed to be variable in the infrared (the YSOVAR survey; Morales-Calderón et al. 2011), and variability in young stellar objects is observed in

[11] See the typical sky spectrum from GTC at http://www.gtc.iac.es/observing/toolbox.php.

Table 5
Fluxes of the Emission Lines Observed in the Two OBs in Protostar #7 (Unreddened Spectra)

Line	OB2 Flux ($\times 10^{-15}$ erg cm^{-2} s^{-1})	OB4 Flux ($\times 10^{-15}$ erg cm^{-2} s^{-1})	OB4/OB2 Ratio
[O I] 5577	0.05	3.7	67.9
[O I] 6300	0.19	1.81	9.7
[O I] 6363	0.04	0.57	15.1
[S II] 6716	NAN	0.97	NAN
[S II] 6731	0.09	2.03	23.4
[Fe II] 7155	0.17	0.77	4.5
[Ca I] 8498	1.38	5.51	4.0
[Ca I] 8452	1.39	5.83	4.2
[Ca I] 8662	1.46	5.41	3.9
[O I] 8446	0.35	1.34	3.8

recent NIR data (Contreras Peña et al. 2014). This variability can be due to several phenomena, such as slow or impulsive variation of the mass accretion rate or of the geometry of the accretion flow; variable shadowing by circumstellar material, which can be associated with a warped disk; stellar rotation with a consequent modulation of the emission observed from the accretion spots that are non uniformly distributed on the stellar surface; and flares arising from magnetic activity (see, for instance, Cody et al. 2014).

OB2 and OB4 observations of protostar #7 were taken four days apart (see Table 2), and significant variability has been observed through comparison of the two epochs, with a flux variation of a factor between two and three in the two OBs. This variability can be compared with the results in Orion from the YSOVAR survey, where the typical peak-to-peak changes in the infrared is about 0.2^m, though with some more extreme cases showing a variability of 1.8^m. Converted into flux unity, these values correspond to variations of a factor 1.2 and 5.2, respectively, similar to what we observed in protostar #7.

The fact that this variability involves not only the continuum from the central object, but also all the emission lines (see Table 5) indicates that it is mainly due to changes in the intensity of the infall/outflow activity. For instance, the CaT lines are more intense in OB4 by a factor of ∼4 compared with OB2, corresponding to an increase in the accretion rate of a factor 3.4. The increase in intensity of all the FELs from OB2 to OB4 indicates that the larger accretion rate in the second day of observation is quickly accompanied by an increase in the intensity of the outflow. Unfortunately, the lack of a detection of the [S II] λ6717 line in the OB2 spectrum does not allow us to estimate the electron density. However, adopting the same N_e found in OB4, we obtain from the OB2 spectra $\dot{M}_{\rm wind} \sim 5 \times 10^{-6}\ M_\odot\ {\rm yr}^{-1}$, which is one order of magnitude smaller than the value observed during the OB4. Variations of similar magnitude have been reported in the literature, such as in the T Tauri star XZ Tau, which showed changes in the intensity of the [O I] λ6300 line by a factor 2.6 in two months (Chou et al. 2013). Variations in the FELs are not the same for all the lines (i.e., Hamann & Persson 1992), suggesting that the observed variability results from a combination of factors.

More surprising is the variability observed in protostar #5. The region around 7500 Å is common in all the three spectra of this source. After dereddening the spectra adopting $A_V = 7.5^m$ (calculated for a 1 Myr old K2 star at the distance of Cyg OB2 using the isochrones from Siess et al. 2000), the flux at 7500 Å in the R100B spectrum is $\sim 9 \times 10^{-15}$ erg cm^{-2} s^{-1} Å, $\sim 7 \times 10^{-14}$ erg cm^{-2} s^{-1} Å in the R2500R and $\sim 1.5 \times 10^{-16}$ erg cm^{-2} s^{-1} Å in the R2500I spectrum. Such variation is greater than the typical variation observed in YSO in recent surveys, such as the Coordinated Synoptic Investigation of NGC 2264, even in bursting stars (Cody et al. 2014; Stauffer et al. 2014). Rapid variations of several magnitudes (the flux variation between the two R2500 spectra roughly corresponds to a magnitude variation of 6.6^m) are usually observed in the FU Orionis stars (Herbig 1966) as a consequence of rapid bursts of mass accretion. This hypothesis is hardly supported, however, by the fact that the decay observed in such stars is longer than the time difference between the two R2500I and R2500R observations (slightly larger than 30 minutes) and by the lack of evidence of a very high mass accretion rate (during the burst in the Fu Ori stars the mass accretion rate increases up to $\sim 10^{-4}\ M_\odot\ {\rm yr}^{-1}$) in the observed spectra. Further observations are required in order to confirm the peculiar variability of this source and rule out the possibility that it can be due to some calibration issue.

7. DISCUSSION

The proplyd-like objects near Cygnus OB2 are unusual and important sources. Evaporating proplyds have already been observed in other young clusters hosting massive stars. Those which have been best characterized are those in the Trapezium in Orion, at distances $d < 0.5$ pc from the O6V star Θ^1 Ori (Bally et al. 1998). The proplyd-like objects near Cyg OB2 have three peculiar characteristics with respect those in the Trapezium: their dimensions (ranging between 18,000 AU and 113,000 AU, while those in Orion are between 40 AU and 400 AU); their distances from the ionizing sources (6–14 pc) and the fact that some of them are thought to host an intermediately massive star in their centers (Comerón et al. 2002).

With the present work, we obtained some insight into the nature of two of the proplyd-like objects in the area surrounding Cygnus OB2: #5 and #7 (Wright et al. 2012). In particular, the central star in object #7 is supposed to be a G star younger than 1 Myr, still in its class I phase (Guarcello et al. 2013); while protostar #5 contains a K2 ± 1 star of similar age. In the optical spectra analyzed here, we found evidence of active accretion in both stars, and both an outflow (with marginal indications for the presence of a stellar jet) and strong variability.

In the case of protostar #7, we derived a mass loss rate $\sim 5 \times 10^{-6}\ M_\odot\ {\rm yr}^{-1}$ in OB2 and $\sim 5 \times 10^{-5}\ M_\odot\ {\rm yr}^{-1}$ in OB4, and mass accretion rate of 1.13–1.17 $\times 10^{-6}\ M_\odot\ {\rm yr}^{-1}$ and 3.8–4.0 $\times 10^{-6}\ M_\odot\ {\rm yr}^{-1}$ in OB2 and OB4, respectively. The mass loss rate is larger than the mass accretion rates, suggesting that the mass evolution in this disk is dominated by the outflow. This is not a common situation in T Tauri stars. For instance, in the sample of 42 T Tauri stars with outflows studied by Hartigan et al. (1995), the mass loss rate are at least one order of magnitude less intense than the mass accretion rate, with the only exception being HN Tau, whose mass loss rate was 0.4 times the mass accretion rate. Other studies, such as Cabrit et al. (1990), indicate that in T Tauri stars typically the mass loss rate is 0.1–0.01 times the mass accretion rate.

The mass loss rate in protostar #7 is particularly intense. In their spectroscopic study of the proplyds in the Orion Nebula Cluster, Henney & Arthur (1998) and Henney & O'Dell (1999) estimated that the mass loss rate of 31 proplyds ranges between $2.5 \times 10^{-8}\ M_\odot\ {\rm yr}^{-1}$ and $1.6 \times 10^{-6}\ M_\odot\ {\rm yr}^{-1}$. This upper limit is about 30 times smaller than the mass loss rate observed in the object #7 during OB4. The absolute values of mass loss rate and mass accretion rate that we derived must, however,

Table 6
Effect of the Extinction on the Used Diagnostics (OB4)

A_V m	Mass Loss Rate ($M_\odot$ yr^{-1})	Mass Accretion Rate ($M_\odot$ yr^{-1})	[O I]/[S II]
6	5.7×10^{-7}	1.7×10^{-8}	0.63
8	2.1×10^{-6}	4.8×10^{-7}	0.94
12	5.0×10^{-5}	3.9×10^{-6}	1.25

be used with caution. The line fluxes have been taken after dereddening the spectra adopting $A_V = 12^m$. This extinction is reasonable if the central protostar is a G star, but this classification is mainly based on the lack of the Paschen series and TiO bands rather than the presence of absorption lines typical of these spectral types. Adopting a different spectral type means that a different value of extinction and stellar parameters in Equation (2) must be used. To verify whether the results of this study are qualitatively consistent and not affected by the uncertainty on stellar extinction, we calculated the mass loss rate, mass accretion rate, and [O I] λ6300/([S II] λ6716 + [S II] λ6731) ratio adopting different values of extinction: $A_V = 0^m$, 6^m, 8^m. The [S II] λ6716/[S II] λ6731 ratio is independent from the adopted extinction. The results are shown in Table 6. The numerical values of mass loss rate and mass accretion rate change adopting different extinctions, but the mass loss rate always exceeds the mass accretion rate.

In the calculation of the mass loss rate and mass accretion rate, we have not taken into account the uncertainty on flux measurement, which is not a trivial task. The main source of flux uncertainty is the fraction of stellar flux that is lost during the observation because of the slit width. This loss is compensated by the flux calibration described in Section 3. To verify whether a less than optimal calibration could affect our result, we can consider the worst case. If the calibration was completely ineffective, given that the upper limit of seeing during the nights of observation is comparable with the slit width (see Table 2) the fraction of stellar flux lost during the observation should be about 50%. Increasing the flux observed in [O I] λ6300 and Ca II λ8542 by this fraction, the mass accretion rate is always smaller than the mass loss rate. We conclude then that our results are not affected by flux calibration uncertainties. Assuming that the flux calibration is reliable, the best estimate on the uncertainty on the flux value can be derived from the signal to noise ratio in the region close to the two lines we used. The OB2 spectra are more noisy than the OB4 ones, and in both OBs the blue part of the spectrum is more noisy than the red part. For [O I] λ6300, an uncertainty between 33% and 50% can be expected on the flux estimate from OB2, and between 14% and 20% in OB4. For the Ca II λ8542 line the expected uncertainties range from 10% to 14% (OB2) and are ∼6% in OB4. Considering these errors and repeating the calculation of the accretion rate and mass loss rate in the two OBs, we find that our estimate of the mass loss rate suffers uncertainty of 40% in OB2 and 16% in OB4, while the estimate of mass accretion rate is uncertain by 8.3% in OB2 and 5.1% in OB4.

One hypothesis concerning the nature of these objects is that they are stars with photoevaporating disks (Wright et al. 2012). While in normal T Tauri stars the mass loss rate is always observed to be about two orders of magnitude less intense than the mass accretion rate, photoevaporating disks are observed with mass loss rates more intense than the mass accretion rates, as observed in σ Orionis (Rigliaco et al. 2009) and the Trapezium (Henney & O'Dell 1999). This characteristic is shared by protostar #7, supporting the hypothesis that the disk in this star is photoevaporating. Furthermore, the O I λ8446 emission line demonstrates the presence of an intense Lyman continuum in the circumstellar environment of #7, and the low [O I] λ6300/([S II] λ6716 + [S II] λ6731) ratio, with a value slightly larger than those typically observed in the ionization fronts of proplyds (Bally et al. 1998; Störzer & Hollenbach 1999), indicates that the environment is characterized by a high level of ionization.

Our data, then, provide strong evidence that the disk in protostar #7 is photoevaporating. However, they do not allow us to differentiate between external or internal driving. The photoevaporation can be externally induced by the UV radiation emitted by the OB stars in the center of Cygnus OB2, which also sculpts the envelope into the typical cometary shape observed in most of the Orion proplyds (Bally et al. 1998). However, the UV radiation field can also be produced by active accretion onto the central star (Gullbring et al. 1998) and the photoevaporation can in this case be "self" induced (Alexander et al. 2006). Without considering the absorption of the UV flux from the intracluster material, the FUV and EUV fluxes emitted by the O stars in Cygnus OB2 are intense enough to induce the observed photoevaporation of the disk in protostar #7. As explained, however, a significant absorption of the EUV photons is expected, mainly by the ionization front in the envelope, while FUV photons can reach and irradiate the disk more easily. To obtain a more quantitative estimate of the absorption of EUV photons, we can combine Equations (5) and (9) in Johnstone et al. (1998) and calculate the ionization radius as:

$$r_{if} = \left(\frac{\dot{M}_{\rm loss}}{12\pi m_H c}\right)^{2/3} \left(\frac{\alpha d^2}{F_{\rm EUV}}\right)^{1/3}, \quad (5)$$

where m_H is the mean particle mass per hydrogen atom; $c \sim 10\,{\rm km\,s^{-1}}$ is the velocity at the ionization radius; $\alpha = 2.6 \times 10^{-13}\,{\rm cm^3\,s^{-1}}$ is the recombination coefficient for hydrogen at $10^4 K$; d is the distance from the ionizing sources and $F_{\rm EUV} = 5.6 \times 10^{50}$ photons s^{-1} is the total emitted EUV flux (summing the emission from all the O stars). Equation (5) gives an ionization radius of 5903 AU (4.″2), which is similar to the distance between the central star and the bright ionization front visible in the IPHAS image (the distance can be understood as an effect of the intracluster absorption of the EUV radiation, which we ignored here). IPHAS images of Cyg OB2 (Vink et al. 2008; Guarcello et al. 2013) show that some residual intracluster gas is still present in the region. This gas can absorb part of the EUV radiation emitted by the O stars in the center of the association before reaching the proplyd-like objects. For instance, an extinction of $A_V = 1.38^m$, which is easy to achieve, is capable of reducing the EUV flux by a factor 100 (calculated from the extinction law of Cardelli et al. 1989). The presence of an ionization front around the central protostar in object #7 and the possibility that part of the EUV radiation is extinguished by the intracluster gas, suggest that the UV radiation created by the accretion process must play an important role in the photoevaporation of the circumstellar disk in this protostar. This is also suggested by the observation of a stronger [O I] λ8446 line during OB4, when the accretion rate was higher. In both scenarios, however, the forbidden emission lines can be produced by the evaporating flow, which is mainly neutral before reaching the ionization front where the EUV radiation is absorbed (Störzer & Hollenbach 1999).

In theory, part of the [O I] λ6300 emission could arise from the disk itself. The proplyds in Orion are in fact also observed

as bright silhouettes in [O I] λ6300 (Bally et al. 1998). Storzer & Hollenbach (1998) have shown that this emission can be produced by the photodissociation front associated with the disks in these photoevaporative systems. This line, in fact, can be excited thermally by collisions if the temperature of the gas in the disk is $T > 3000$ K, which is possible when the disk is illuminated by FUV radiation with an intensity of 10^3–10^4 G_0. Also a non-thermal component due to the dissociation of OH molecules can be present (Störzer & Hollenbach 2000). However, the emission from the disk should be symmetrical, broadened by the Keplerian velocity of the disk, and centered on λ = 6300 Å. We do not observe such a broadened component in the [O I] λ6300 profile in the spectra of protostar #7, suggesting that it is absent or much weaker than the blueshifted component due to the outflow.

8. CONCLUSIONS

We have analyzed optical low-resolution spectra taken with OSIRIS@GTC of two candidate photoevaporating disks in the area surrounding the massive association Cygnus OB2. These candidate photoevaporating protostars were recently discovered by Wright et al. (2012) and some have also been found to host T Tauri stars with disks (Guarcello et al. 2013).

One of the two targets, protostar #5, hosts a K2 ± 1 star, using nomenclature by Wright et al. (2012). Its young age is demonstrated by the presence of a Li λ6708 absorption line and evidence of active accretion. Its spectra do not show any emission feature related to intense outflow but allow us to classify the central object as an actively accreting T Tauri star.

The spectra of the other target, object #7, do not show absorption features that allow an accurate spectral classification. We adopted a G spectral type based on the lack of Paschen series and TiO bands in the observed spectra. The spectra of this star, taken in two different nights of observations, are characterized by the presence of several emission lines that allow us to study the nature of this peculiar object. The main results are as follows.

1. The [O I] λ6300/([S II] λ6716 + [S II] λ6731) ratio is typical of environments with a high level of ionization, such as H II regions irradiated by O stars, and the presence of the O I λ8446 line is typical of environments with intense local UV field.
2. A strong Ca II triplet is observed with a saturated 8498:8542:8662 Å flux ratio typical of optically thick emission. The mass accretion rate estimated from the luminosity of the Ca II λ8542 line is typical of intense accretors.
3. The presence of FELs demonstrates that the star is characterized by outflow. The asymmetric profile seen in some of the FELs can be explained by a superposition of high-velocity (∼400 km s^{-1}) and low-velocity (⩽100 km s^{-1}) components typical of the presence of both disk wind and stellar jet.
4. The [S II] λ6716/[S II] λ6731 ratio is in the saturated regime, corresponding to an electron density in the outflow of $\log(N_e) = 4.03$ cm^{-3}.
5. We derived a high mass loss rate from [O I] λ6300 and [S II] λ6731.
6. Both sources show large amplitude and rapid variability both in the continuum and the intensity of the emission lines. In object #7, we find evidence suggesting that the variability is due to a rapid increase of infall/outflow activity.

We find that in protostar #7, the mass loss rate is higher than the mass accretion rate, which is a characteristic of evaporating disks. This result is also supported by the comparison with the well-studied proplyds in Orion, the high level of ionization and the intense local UV field in the circumstellar environment. Even if our data do not allow us to differentiate between the scenarios in which the photoevaporation is externally induced by the OB stars in the center of Cygnus OB2 or self-induced by the central star itself, with the luminous Lyman continuum produced by the accretion shocks at the stellar surface, our study clearly indicates that the disk in protostar #7 is photoevaporating as a consequence of intense incident UV radiation.

We thank the anonymous referee who helped us to significantly improve the quality of this manuscript. This paper is based on observations made with the Gran Telescopio Canarias (GTC), installed in the Spanish Observatorio del Roque de los Muchachos of the Instituto de Astrofísica de Canarias, on the island of La Palma. This paper is also based on data from the IPHAS and SDSS Data Release 9. The IPHAS survey has been carried out at the INT. The INT is operated on the island of La Palma by the Isaac Newton Group in the Spanish Observatorio del Roque de los Muchachos of the Instituto de Astrofísica de Canarias. Funding for SDSS-III has been provided by the Alfred P. Sloan Foundation, the Participating Institutions, the National Science Foundation, and the U.S. Department of Energy Office of Science. M.G.G. was supported by Chandra grant GO0-11040X during the course of this work. J.J.D. was funded by NASA contract NAS8-03060 to the Chandra X-ray Center and thanks the Director, Belinda Wilkes, for continuing support. M.G.G. also acknowledges grant PRIN-INAF 2012 (PI: E. Flaccomio).

REFERENCES

Adams, F. C., Hollenbach, D., Laughlin, G., & Gorti, U. 2004, ApJ, 611, 360
Alexander, R. D., & Armitage, P. J. 2006, ApJL, 639, L83
Alexander, R. D., Clarke, C. J., & Pringle, J. E. 2006, MNRAS, 369, 216
Allen, L. E., & Strom, K. M. 1995, AJ, 109, 1379
Appenzeller, I., & Wolf, B. 1977, A&A, 54, 713
Bally, J., Sutherland, R. S., Devine, D., & Johnstone, D. 1998, AJ, 116, 293
Balog, Z., Muzerolle, J., Rieke, G. H., et al. 2007, ApJ, 660, 1532
Balog, Z., Rieke, G. H., Su, K. Y. L., Muzerolle, J., & Young, E. T. 2006, ApJL, 650, L83
Barentsen, G., Vink, J. S., Drew, J. E., et al. 2011, MNRAS, 415, 103
Beerer, I. M., Koenig, X. P., Hora, J. L., et al. 2010, ApJ, 720, 679
Bowen, I. S., & Swings, P. 1947, ApJ, 105, 92
Brandner, W., Grebel, E. K., Chu, Y.-H., et al. 2000, AJ, 119, 292
Cabrit, S., Edwards, S., Strom, S. E., & Strom, K. M. 1990, ApJ, 354, 687
Calvet, N., & Gullbring, E. 1998, ApJ, 509, 802
Calvet, N., Hartmann, L., & Strom, S. E. 2000, Protostars and Planets IV (Tucson, AZ: Univ. Arizona Press), 377
Cardelli, J. A., Clayton, G. C., & Mathis, J. S. 1989, ApJ, 345, 245
Cepa, J., Aguiar, M., & Escalera, E. A. 2000, Proc. SPIE, 4008, 623
Chou, M.-Y., Takami, M., Manset, N., et al. 2013, AJ, 145, 108
Cody, A. M., Stauffer, J., Baglin, A., et al. 2014, AJ, 147, 82
Comerón, F., Pasquali, A., Rodighiero, G., et al. 2002, A&A, 389, 874
Contreras Peña, C., Lucas, P. W., Froebrich, D., et al. 2014, MNRAS, 439, 1829
Czyzak, S. J., Keyes, C. D., & Aller, L. H. 1986, ApJS, 61, 159
Drew, J. E., Greimel, R., Irwin, M. J., et al. 2005, MNRAS, 362, 753
Edwards, S., Hartigan, P., Ghandour, L., & Andrulis, C. 1994, AJ, 108, 1056
Elmegreen, B. G. 2011, in EAS Publications Series, Vol. 51, Star Formation in the Local Universe, ed. C. Charbonnel & T. Montmerle (Cambridge: Cambridge Univ. Press)
Fang, M., van Boekel, R., King, R. R., et al. 2012, A&A, 539, A119
Fedele, D., van den Ancker, M. E., Henning, T., Jayawardhana, R., & Oliveira, J. M. 2010, A&A, 510, A72
Grandi, S. A. 1975, ApJ, 196, 465
Grandi, S. A. 1980, ApJ, 238, 10

Griffith, M., Heflin, M., Conner, S., Burke, B., & Langston, G. 1991, ApJS, 75, 801
Guarcello, M. G., Drake, J. J., Wright, N. J., et al. 2013, ApJ, 773, 135
Guarcello, M. G., Micela, G., Damiani, F., et al. 2009, A&A, 496, 453
Guarcello, M. G., Micela, G., Peres, G., Prisinzano, L., & Sciortino, S. 2010, A&A, 521, A61
Guarcello, M. G., Prisinzano, L., Micela, G., et al. 2007, A&A, 462, 245
Guarcello, M. G., Wright, N. J., Drake, J. J., et al. 2012, ApJS, 202, 19
Gullbring, E., Hartmann, L., Briceno, C., & Calvet, N. 1998, ApJ, 492, 323
Gutermuth, R. A., Myers, P. C., Megeath, S. T., et al. 2008, ApJ, 674, 336
Habing, H. J. 1968, BAN, 19, 421
Haisch, K. E., Jr., Lada, E. A., & Lada, C. J. 2001, ApJL, 553, L153
Hamann, F. 1994, ApJS, 93, 485
Hamann, F., & Persson, S. E. 1992, ApJS, 82, 247
Hartigan, P., Edwards, S., & Ghandour, L. 1995, ApJ, 452, 736
Hartmann, L., Calvet, N., Gullbring, E., & D'Alessio, P. 1998, ApJ, 495, 385
Henney, W. J., & Arthur, S. J. 1998, AJ, 116, 322
Henney, W. J., & O'Dell, C. R. 1999, AJ, 118, 2350
Herbig, G. H. 1966, VA, 8, 109
Herbig, G. H., & Soderblom, D. R. 1980, ApJ, 242, 628
Hernández, J., Calvet, N., Briceño, C., Hartmann, L., & Berlind, P. 2004, AJ, 127, 1682
Hernández, J., Hartmann, L., Megeath, T., et al. 2007, ApJ, 662, 1067
Hester, J. J., Scowen, P. A., Sankrit, R., et al. 1996, AJ, 111, 2349
Hirth, G. A. 1994, in ASP Conf. Ser. 57, Stellar and Circumstellar Astrophysics, a 70th birthday celebration for K. H. Bohm and E. Bohm-Vitense, ed. G. Wallerstein & A. Noriega-Crespo (San Francisco, CA: ASP), 32
Hirth, G. A., Mundt, R., & Solf, J. 1997, A&AS, 126, 437
Jeffries, R. D., & Oliveira, J. M. 2005, MNRAS, 358, 13
Johansson, S., & Letokhov, V. S. 2005, MNRAS, 364, 731
Johnstone, D., Hollenbach, D., & Bally, J. 1998, ApJ, 499, 758
Kastner, S. O., & Bhatia, A. K. 1995, ApJ, 439, 346
Kepner, J., Hartigan, P., Yang, C., & Strom, S. 1993, ApJL, 415, L119
Koenig, X. P., Allen, L. E., Kenyon, S. J., Su, K. Y. L., & Balog, Z. 2008, ApJL, 687, L37
Kwan, J. 1997, ApJ, 489, 284
Kwan, J., & Fischer, W. 2011, MNRAS, 411, 2383
Kwan, J., & Tademaru, E. 1988, ApJL, 332, L41
Lada, C. J., Muench, A. A., Luhman, K. L., et al. 2006, AJ, 131, 1574
Mamajek, E. E. 2009, in AIP Conf. Proc. 1158, Exoplanets and Disks: Their Formation and Diversity, ed. T. Usuda, M. Tamura, & M. Ishii (Melville, NY: AIP), 3
Martins, F., Schaerer, D., & Hillier, D. J. 2005, A&A, 436, 1049
Mathew, B., Banerjee, D. P. K., Subramaniam, A., & Ashok, N. M. 2012, ApJ, 753, 13
McCaughrean, M. J., & Andersen, M. 2002, A&A, 389, 513
Morales-Calderón, M., Stauffer, J. R., Hillenbrand, L. A., et al. 2011, ApJ, 733, 50
Münch, G., & Taylor, K. 1974, ApJL, 192, L93
Muzerolle, J., Hartmann, L., & Calvet, N. 1998, AJ, 116, 455
Natta, A., Testi, L., Muzerolle, J., et al. 2004, A&A, 424, 603
Parravano, A., Hollenbach, D. J., & McKee, C. F. 2003, ApJ, 584, 797
Pereira, C. B., & Miranda, L. F. 2007, A&A, 462, 231
Proxauf, B., Öttl, S., & Kimeswenger, S. 2014, A&A, 561, A10
Randich, S., Bragaglia, A., Pastori, L., et al. 2005, Msngr, 121, 18
Rigliaco, E., Natta, A., Randich, S., & Sacco, G. 2009, A&A, 495, L13
Robitaille, T. P., Whitney, B. A., Indebetouw, R., & Wood, K. 2007, ApJS, 169, 328
Rygl, K. L. J., Brunthaler, A., Sanna, A., et al. 2012, A&A, 539, A79
Siess, L., Dufour, E., & Forestini, M. 2000, A&A, 358, 593
Smith, N., Bally, J., & Morse, J. A. 2003, ApJL, 587, L105
Solf, J. 1989, in ESO Conf. Proc. 33, Low-Mass Star Formation and Pre-Main-Sequence Objects, ed. B. Reipurth (Garching: ESO), 399
Stauffer, J., Cody, A. M., Baglin, A., et al. 2014, AJ, 147, 83
Stecklum, B., Henning, T., Feldt, M., et al. 1998, AJ, 115, 767
Storzer, H., & Hollenbach, D. 1998, ApJL, 502, L71
Störzer, H., & Hollenbach, D. 1999, ApJ, 515, 669
Störzer, H., & Hollenbach, D. 2000, ApJ, 539, 751
Strelnitski, V., Bieging, J. H., Hora, J., et al. 2013, ApJ, 777, 89
Throop, H. B., & Bally, J. 2005, ApJL, 623, L149
Torres-Dodgen, A. V., & Weaver, W. B. 1993, PASP, 105, 693
Uchida, Y., & Shibata, K. 1984, PASJ, 36, 105
Vink, J. S., Drew, J. E., Steeghs, D., et al. 2008, MNRAS, 387, 308
Walborn, N. R., & Fitzpatrick, E. L. 1990, PASP, 102, 379
Whelan, E. T., Ray, T. P., & Davis, C. J. 2004, A&A, 417, 247
Whitworth, A. 1979, MNRAS, 186, 59
Wiese, W. L., Smith, M. W., & Miles, B. M. 1969, Atomic transition probabilities. Vol. 2: Sodium through Calcium. A critical data compilation (Washington, DC: US Department of Commerce, National Bureau of Standards)
Wright, N. J. 2014, ApJ, in press
Wright, N. J., Drake, J. J., Drew, J. E., & Vink, J. S. 2010, ApJ, 713, 871
Wright, N. J., Drake, J. J., Drew, J. E., et al. 2012, ApJL, 746, L21
Wright, N. J., Parker, R. J., Goodwin, S. P., & Drake, J. J. 2014, MNRAS, 438, 639
Yusef-Zadeh, F., Biretta, J., & Geballe, T. R. 2005, AJ, 130, 1171